Direct observation at the microscale of particle deposition during the first stage of the microfiltration process

Alberto Valencia, Claude Le Men, Christophe Ellero, Christine Lafforgue-Baldas, Philippe Schmitz, Jeffrey F. Morris

Direct observation at the microscale of particle deposition during the first stage of the microfiltration process

Alberto Valencia[a]* · Claude LeMen[b] · Christophe Ellero[b] · Christine Lafforgue-Baldas[b] · Philippe Schmitz[b] · Jeffrey F. Morris[c] ·

[a)] FERMAT, Université de Toulouse, INSA, TBI, Avenue de Rangueil, 135, F-31077 Toulouse, France

*Corresponding author:

E-mail address: valencia@insa-toulouse.fr (A.Valencia)

Tel : +33 5 61 55 97 70

[b)] Université de Toulouse, INSA, TBI, Avenue de Rangueil, 135, F-31077 Toulouse, France

[c)] Levich Institute and Dept. of Chemical Engineering, CUNY City College of New York, 140th Street and Convent Avenue, New York, NY 10031

Abstract

Particle deposition at pore scale during membrane filtration has been studied. A specially designed microfiltration set-up, including a filtration membrane composed of slots alignment, was used to perform *in-situ*, real time measurements of the particle concentration and cake growth during filtration of spherical latex particles. The approach allows the microscale phenomena to be related to macroscopic features. The measurements were obtained by direct observation from the side, using video imaging. A dedicated image processing code was developed to analyze the filtration imaging; cake growth monitoring as well as particle tracking and velocimetry are performed using this tool. The image analysis combined with pressure measurements allowed a thorough evaluation of system performance, and has proven effective for filtration analysis of more complex suspensions. The membrane geometry was shown to have a pronounced influence on the formation of the first deposited layers, and this effect persists throughout the later cake growth for the model micro-particles.

Keywords: Micro-filtration · Membrane fouling · Cake formation · Microsystem · Pore protection

1 Introduction

Membrane filtration as a separation process is widely used in many industries and various other human activities [1]–[4]. To optimize performance, it is natural to seek effective solutions to filtration and separation problems [5]. One important hindering feature regarding membrane filtration is the fouling phenomenon, which is mainly related to particle accumulation and the consequent permeate flux decline [6]. Various approaches have been explored to overcome these issues. Some of the current research topics are: membrane surface modification, the flow hydrodynamic conditions, the geometry and membrane reconditioning. The work of Xue et al. [7] provides guidance to an efficient method for improvement of membrane wettability and water flux, through surface coating and mineralization. The potential for improvement based on alteration of the hydrodynamic conditions has been studied as well [8]. Different geometries change the flow patterns and may induce larger shear stress, a factor that tends to hinder cake formation. Studies have also been made to elucidate how filtration parameters may be varied to optimize the process. Pressure step changes have been shown to have an influence on the cake structure of kaolin slurry and nanosilica sol [9]. When the pressure is increased stepwise, the cake structure at the initial pressure tends to approach that of a cake formed under the later pressure; nonetheless in the case of stepwise pressure decrease, the initial compressed cake does not expand to the corresponding later pressure state. In addition, to avoid cake build-up, methods to clean and recondition the membrane performance to its initial state are major research topics [10], [11].

Other approaches addressing cake structure and the influence of particle interactions have been applied in order to better understand the mechanism involved in the filtration phenomenon [12], [13]. The use of laser triangulometry gave an important breakthrough for in-situ non-invasive data acquisition; however, there remains a need to enhance resolution of this method. Understanding the filtration mechanisms at the microscale is crucial for process optimization and hardware design, as well as to model the cake structure, morphology and porosity

distribution to predict filtration performances under different operating conditions. Direct observation techniques are especially valuable in this regard, as these allow in-situ, non-invasive data acquisition. The direct observation through membrane (DOTM) experimental approach, first proposed by Hodgson et al. [14] and further developed by Li et al. [15], has been used to observe particle deposition on the membrane surface during crossflow microfiltration, in work which considered flowrates both below and above the critical flux. The main drawbacks of this technique remain the limited optical depth and the focal plane of the observation. The configuration used by Li et al. allows observation of the top of the cake, which is convenient to study the fractional membrane coverage but is less suited for probing other cake properties. Inspired by this experimental configuration, Zhang et al. [16] developed a mass balance method combined with the direct observation technique using image processing. This method gave a more accurate representation of deposition of particles. The DOTM technique has also been coupled with confocal laser scanning microscopy (CLSM), which uses the fluorescence principle to obtain 3D information at different depths of the studied sample. The work by Ben Hassan et al. [17] characterized particle deposition and cake structure using laser excitation and fluorescent cells and particles. The pore protection phenomenon and its dependence on membrane geometry were observed. The main drawback of this technique is that it relies on the very thin optical depth associated with the laser penetration. This limits the observable cake thickness and requires the filtration to be run stepwise, which yields a non-continuous analysis. The 2007 study by Le Clech et al. [18] used direct observation from the side to study fouling formation on a hollow fiber membrane. This configuration revealed a concentration gradient during filtration deposition of alginate/bentonite solution, but the resolution of the acquired images did not allow examination at the particle level. More recent work by Laar et el. [19] used direct observation of clogging phenomenon in dead-end filtration. They used different membrane configurations and coupled the observation with particle image velocimetry (PIV); this work showed it was possible to provide insight on the flow through the pores and its effect on particle clogging mechanisms.

In this paper the focus is on the validation of a new microsystem for characterizing the fouling phenomenon in filtration and particularly cake properties using the direct observation from the side. The system allows the *in-situ* real-time acquisition of images, from which the concentration field and mean velocity were estimated. This system operates under dead-end filtration condition. This approach is accurate for analyzing the first layers of cake and the first stage of cake formation; even under crossflow operation conditions it is well known that some particles accumulate at the membrane surface as the flow direction in the vicinity of the membrane is perpendicular to the filtration surface [20]. In addition, dead-end operating condition is particularly adequate for performing the mass balance, which is the basis of the further quantitative analysis. The mass balance has been a source of uncertainty in previous studies on crossflow operation mode, which pointed out the difficulty to assess the deposited mass thorough the filtration [21].

The designed filtration membrane is composed of consecutives slots aligned with different spacing obtained by plasma photo-etching. The system has been validated by analyzing the behavior of rigid spherical particle suspension near the membrane during the early stages of membrane blocking, deposition of the first cake layers, and the transition to a fully-developed cake. Particle deposition in the early filtration is studied for different membrane geometries and its effect in later cake growth is examined and compared to other studies of the literature. The cake first layers structure is qualitatively described and then simulated to compare the simulation results with the experimental measurements. The analysis method using image processing is explained and results obtained for model micro particles are discussed.

2 Materials and methods

2.1 Experimental set-up and protocol

An original direct observation (DO) experimental set-up was constructed so that particle deposition could be characterized in-situ and in real time from the side. Micro-filtration cells were specially designed and crafted using photolithography and plasma etching techniques in collaboration with the laboratory LAAS (Laboratoire d'Analyse et d'Architecture des Systèmes). The dead-end filtration cell consists of a straight channel with a filtering structure at the middle. This structure is composed of consecutive slots arranged in different configurations (Fig. 1). These configurations were selected to explore the effect of slot width and distance (miming pore size and pore density in usual membranes) on permeability and cake formation : C is the slot width and Pe is the slot distance that is related to slot periodicity or pore density. The channel is 11.5 mm long, 1 mm in width and 30 µm in depth. Finally, the cell is covered with a glass slip of 170 µm thickness allowing *in-situ* observation.

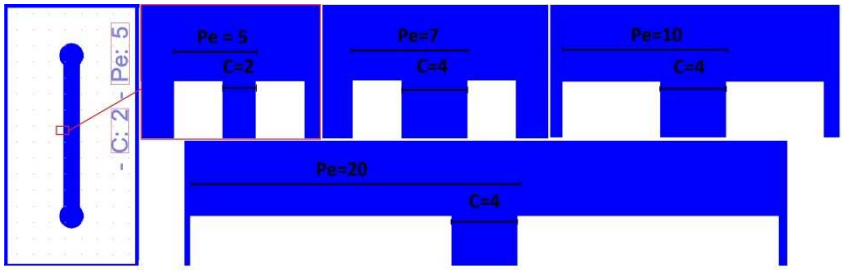

Fig. 1 Microfiltration cell configurations. Left figure represents the channel configuration with the filtration cell in the middle. The inlet is at the top and outlet at the bottom of the channel. Highlighted at right: zoom view of the corresponding cell membrane, C2Pe5 (units in µm) and the other different geometries.

Table 1. Microfiltration cell geometries

Membrane reference	Slot width, C (µm)	Periodicity, Pe (µm)	Slot distance d_p wall (µm)
C2Pe5	2	5	3
C4Pe7	4	7	3
C4Pe10	4	10	6
C4Pe20	4	20	16

The very fine microstructure of the membrane for C2Pe5 and C4Pe7 units was an important challenge as the finest walls of the membrane (pore distance) are 3 µm wide and 30 µm deep, conditions for which the plasma etching becomes more difficult to perform and the wall structure is more fragile.

A microscope objective attached to a camera (Basler acA 1920-155µm) is used for real-time imaging and data acquisition (Fig. 2a). A syringe pump (Harvard Apparatus 33) provides suspension flow-rates in the range of 1 to 20 µl/min resulting in linear velocity of 0.5 - 15 mm/s at the filter. A digital pressure gauge (Type E2 - Sika) is used to measure pressure.

A 78.9% water - 21.1% glycerin mixture (by volume) is used as suspending fluid to match the particle density of 1.055 g/cm^3 and provide neutrally buoyant condition. In order to avoid the presence of dust particles in the system, the water-glycerin solution is filtered (0.2 µm pore diameter). Before preparing the suspension, dissolved gas is extracted from solution and the suspension prior to each experiment to avoid the formation of gas bubbles due to pressure drop when the fluid passes through the membrane; a vacuum pump (Knf, Laboport) is used for this purpose. After dust and dissolved gas are removed, the system is filled with water-glycerin mixture and characterized for the pure fluid flow. After the stationary flow condition is reached, the particle suspension is injected. The filtration starts and real-time imaging and data acquisition is launched when the first particles arrive to the observation field.

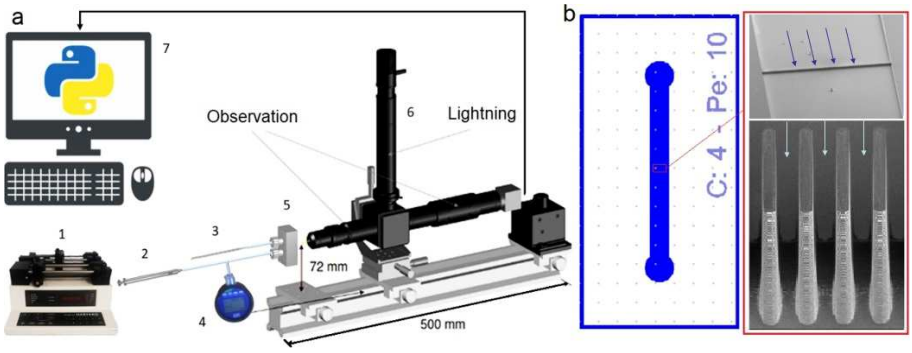

Fig. 2 a) Scheme of the experimental set-up. 1) Syringe pump, 2) Syringe, 3) Reservoir, 4) Manometer, 5) Cell support, 6) Optical bench 7) Acquisition computer. b) Detail of the microfiltration cell, design and SEM observation.

The choice of the camera frame rate is in agreement with range of velocities related to the flowrate. Working on low Reynolds number conditions (< 1), Stokes flow is assumed. As it is intended to study the actual

particle deposition it is compulsory to have an acquisition rate fast enough to capture particle movement. The neutrally buoyant condition of the experiments made gravity and inertial forces negligible relative to viscous forces. This results in particles following closely the streamlines with negligible relative (slip or migration) velocity to the fluid.

2.2 Particle suspension

The suspension used for the experiments consists of latex beads (Micro Particles GmbH PS-R-8.4) of mean diameter d_p = 8.4 µm and standard deviation 0.09 µm suspended in the noted water –glycerin mixture. The concentration C ~ 0.1% (V/V) is according to the clogging capacity of the system and the duration of the experiments.

2.3 Image processing

A specialized Python code is used to analyze the acquired images. This code is based on three modules: the particle velocimetry module (PVM), the particle concentration module (PCM), and the cake growth monitoring module (CGM). All modules use an identification function and a dedicated algorithm to extract the desired information, namely the velocity, concentration or the deposited mass.

The identification function detects contours and allows assessment of their properties. The size, shape and the position of an identified object are used to differentiate the particles from the cake. These parameters are calibrated for a sample of 100 objects in order to determine the best fit. For both particles and the cake, the image is first binarized and voids are filled to allow the contours to be better identified. Having the contours and the properties of the detected objects, filters are applied to classify them and to perform the analysis (Fig. 3).

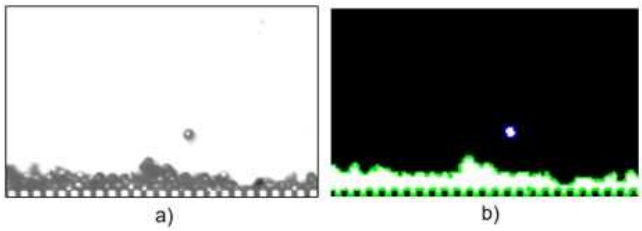

Fig. 3 a) Raw image of a particle approaching the membrane in a filtration experiment. b) Particle (blue) and cake (green) identification after binarizing and filling.

The PCM identifies particles above the cake zone, allowing calculation of the vertical concentration profile and the instantaneous mean concentration in the imaged zone. The PVM goes beyond identification by using a correlation function to track particle trajectories. This correlation function is also used to calculate the mean velocity from the displacement of the vertical concentration profile in the time-lapse of two consecutive images. This information allows analyzing the cake growth (surface, mean height, heterogeneity) and correlate it to particle concentration and velocity.

2.3.1 Cake growth monitoring module

After contours are identified, the CGM uses the position filter to classify a contour as part of the cake. When the cake is found, the coordinates of the surface are extracted and then the cake mean height and heterogeneity are determined.

2.3.2 Particle concentration module

Once the contours are classified, there are two approaches to calculate the concentration. In the first the number of contours is related to individual spherical particles which have an associated volume. Then dividing the particles cumulative volume by the channel volume provides an estimate of the concentration. The second approach consists of inspecting each pixel line and evaluating the particle presence as a 1D signal. Then this 1D information is transformed into a spherical particle cross section. The ratio of pixels occupied by particles to the total number of pixels in the cross section to channel cross section yields a measure of the vertical concentration profile.

2.3.3 Particle velocimetry module

For the PVM the algorithm is developed according to previous studies [22], [23]. This function allows tracking several particles at consecutive instants and hence re-constructing their individual trajectories. Knowing the time interval Δt between acquisition of sequential images, it is also possible to calculate particle velocities.

For this purpose, the image fraction corresponding to the individual particle is extracted as a reference matrix *R(N,N)* determined from the image pixel values. Then the image fraction of the particle vicinity at the immediately next image is also extracted in a target matrix *T(M,M)*. The autocorrelation matrix is then calculated for *R(N,N)* and *T(M,M)*:

$$S(i,j) = \sum_{x,y=0}^{M-N} |T(i+x, j+y) - R(x,y)|$$

Eq. 1

The minimum value of the correlation matrix reveals the position *(i,j)* of *R* in *T* that corresponds to the coordinate of the particle in the immediately next instant. This algorithm is designed to characterize flow irregularities and heterogeneity in membrane permeability.

However, while individual tracking of particles is possible, it could take long calculation time. This method is mainly used to study particle trajectories when a preferential flow in a certain zone of the membrane is observed. Another approach to study flow is based on the vertical concentration profile calculated previously using the PCM. The correlation between the concentration profiles of two consecutive images is used to determine the velocity at which the concentration front is driven towards the cake. This provides an estimation of the mean velocity. For each method, a sampling is done to compare the code results to the values calculated directly from the images.

2.4 Data analysis

From the concentration obtained from the images as the volume represented by the particles identified within the observation window to the corresponding channel volume the mass balance can be established. Comparing the observed cake height using the CGM, to the integration of the concentration extracted by the PCM.yields:

$$\frac{\int QC\, dt}{(1-\epsilon_h)\, S} = \bar{h}_o$$

Eq. 2

where Q (µm³/s) is the flow rate, C (% V/V) the concentration computed using the PCM, S (µm²) the area of the channel cross section, ϵ_h the porosity and the right side of the equation corresponds to the mean height of the forming cake obtained using the CGM. The porosity ϵ_h is obtained fromEq. 2, in which it is the only unknown parameter. Then the porosity previously found is compared to the one obtained from the analysis of the pressure data using the Kozeny-Carman expression for the cake resistance in Darcy's law,

$$\frac{Q}{S} = \frac{\Delta P}{\mu\left(R_m + \frac{\bar{h}_o K S_p^2 \left(1-\epsilon_{h,p}\right)^2}{{\epsilon_{h,p}}^3}\right)}$$

Eq. 3

with *ΔP (Pa)* the trans-membrane pressure, μ (Pa·s) the dynamic viscosity, R_m (m^{-1}) the membrane hydraulic resistance, $\bar{h}_o$ (m) the cake mean height, S_p (m^{-1}) the specific surface of the particles, ϵ the porosity and $K_K = 5$ for spherical particles [24]. The term in parentheses corresponds to the total hydraulic resistance model $R_t = R_m + R_c$. This approach is accurate since the whole channel depth remains within the optical scope of observation, and hence the information lost in depth when calculating the concentration and the cake height remains negligible.

2.5 Numerical simulations

In order to characterize the hydrodynamics in the system and the cake building process the system was analyzed using the commercially available finite element code COMSOL Multiphysics™. The simulations are focused on the microfiltration cell performance as well as the early behavior of the cake formation. The stationary laminar flow of pure fluid was solved for the (i) entire system without the membrane, (ii) with the membrane and (iii) the membrane-cake interaction simplified geometry (Fig. 4).

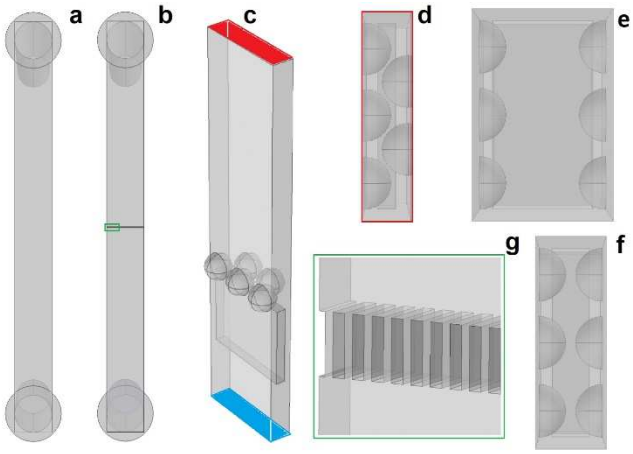

Fig. 4 a) Front view of the channel geometry without the membrane (Suspension inlet at the top of the channel and permeate outlet at the bottom of the channel). b) Complete geometry of the channel with the membrane. c) 3D simplified geometry for cake-membrane interaction (for C4Pe7 membrane). d,e,f) Top-view of the simplified geometry C4Pe7, C4Pe20, C4Pe10 respectively. g) Detail on the membrane simulated geometry, example for a C4Pe10 unit.

These geometries were studied in order to analyze the different contributions to the total pressure drop in the system: the channel alone (Fig. 4a), the channel-membrane (Fig. 4b) and the membrane blocking geometry (Fig. 4c); these were also related to the hydraulic resistance contributions from the Darcy equation R_m and R_c. The geometry for the membrane-cake interaction when the first particles arrive was simulated based on the real observation of the slot blocking configurations depending on the different membrane geometries (Fig. 1) and supposing an optimal membrane coverage. The stationary laminar flow was simulated in order to find the pressure drop and the individual hydraulic resistance for comparing to the experimental values.

2.5.1 Initial conditions

A reference pressure of 0 Pa is set at the outlet (blue zone in Fig. 4c). The initial velocity is calculated based on the experimental flow rate of 10 µl/min divided by the corresponding channel section and set as the normal velocity at the inlet (red zone in Fig. 4c). The fluid is set as 20° C water/glycerin mixture and has a density of 1060 kg/m^3 and a viscosity of 2.0E-3 Pa.s.

2.5.2 *Flow model*

The Navier-Stokes equations simplified to the Stokes equations for the laminar regime Re<<1 are considered for the simulations. The three dimensional domain (Fig. 4) is modeled taking into account the wall effects as the channel depth is small. Navier-Stokes momentum and continuity equations are simplified to:

$$0 = -\nabla p + \nabla.\left(\mu(\nabla u + (\nabla u)^T)\right)$$
$$\nabla.u = 0$$

Eq. 4

with p is the pressure and u the flow velocity

The boundary conditions (Fig. 4a and b) were set as no slip on the walls, along with the inlet and the outlet conditions. For the membrane-cake interaction from the top view in Fig. 4d, the bottom and top boundaries (edges) were considered walls while the side boundaries were considered symmetric to simulate a periodic domain. This is a fair assumption as the membrane length ratio to the channel depth is much larger than unity. The inlet corresponds to the red highlighted surface at the top and the outlet corresponds to the bottom blue surface in Fig. 4c.

3 Results and discussion

The strategy described was used in filtration experiments to characterize the system and study the influence of membrane geometry on cake construction. From the instantaneous mean height of the cake, mean concentration above the cake surface and the particle-flow velocity it is possible to monitor the cake growth, perform a mass balance and describe the cake structure related to the porosity. The permeability and the Kozeny coefficient of the resulting deposits are analyzed. Using Eq. 3 the estimated porosity is checked.

3.1 Qualitative analysis

The first stages of the filtration exhibit behavior strongly dependent on the membrane geometry. As shown in Fig. 5, after the first particles reach the membrane, the relation between the particle diameter and the slot distance induces different particle cake structures. The characteristic Stokes flow corresponds to $Re < 1$ [25] which is the case for the filtration experiments. The viscous forces are higher than the inertial forces; as a result, particles in the dilute suspension follow closely the fluid flow streamlines with negligible particle-fluid relative velocities. Consequently, particles are guided by the flow and they flow preferentially to the slots. The slot distribution plays a role in the in the organization of the particles in the first layers; once the slots are blocked, the following particles approaching a blocked slot are driven to the membrane surface zone corresponding to the walls separating the slots. Depending on the distance between slots, a certain number of particles can deposit on these zones, causing the particles to arrange differently in order to fill the whole membrane surface.

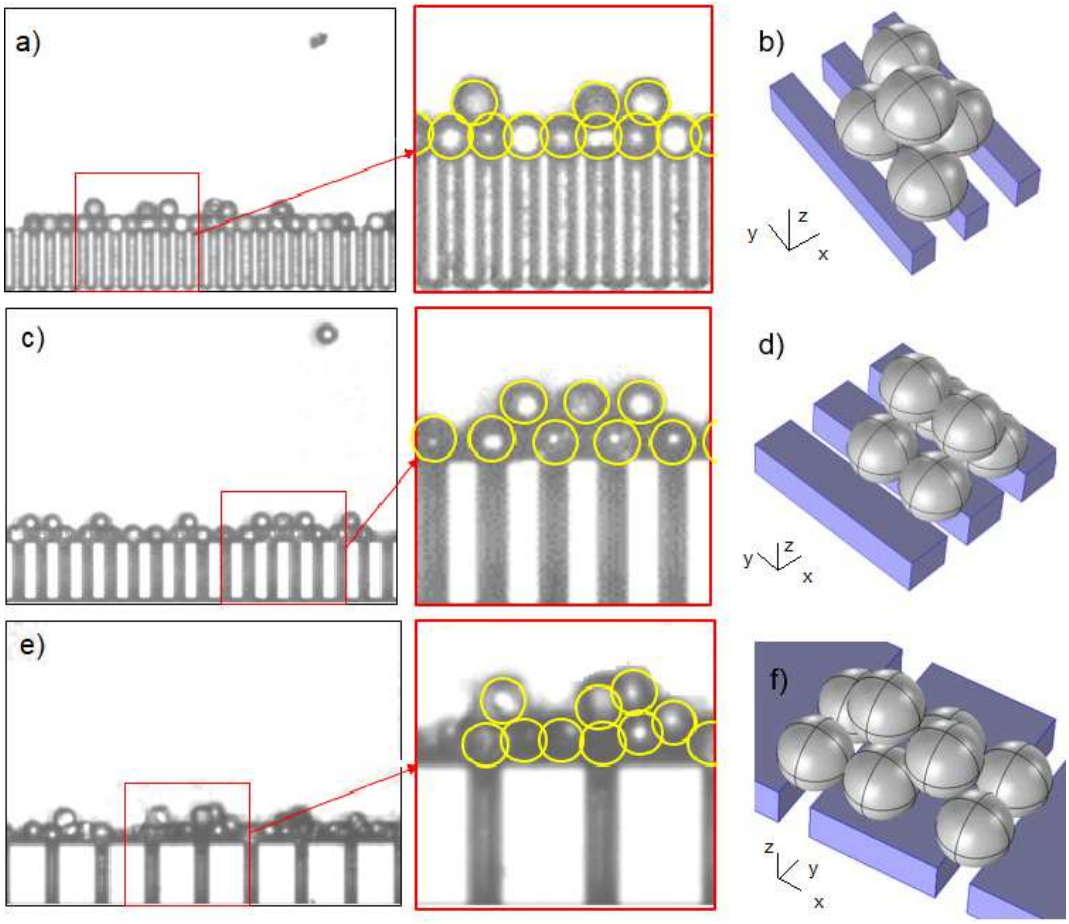

Fig. 5 a,c,e) First stage of cake formation for C4Pe7, C4Pe10 and C4Pe20 configurations, respectively. b,d,f) Sketches of the typical structure of particle arrangement for the corresponding membrane configuration

For C4Pe7 units, d_p is small compared to the diameter of the particles (8.4 µm) and the slot width is $C = 4$ µm; with $d_p = 3$ µm, particles are not able to lay on the walls, moreover d_p is too small and their arrangement results in a moderate slot blocking since they cannot be closely aligned over a slot. According to this arrangement, particles centers are not aligned on the same axis following the membrane length direction (x), hence causing a shift of the particles in the depth direction (y). This causes the overlaying highlighted by the circles in Fig. 5a, as some particles are displaced in y, some of them cannot be observe in the focus plane. Fig. 5b illustrates the previous analysis: for the C4Pe7 configuration, particles are spread over all the membrane with large spaces between each other and in a limited depth, thus large voids are formed in the first layers resulting in high porosity. This phenomenon has been reported as the pore protection phenomenon and it yields a more porous blocking layer [17]. The membrane blocking remains moderate and this slot configuration induces a pyramidal arrangement as it is possible to see in Fig. 5a and b.

In the case of C4Pe10 $d_p = 6$ µm which corresponds almost to the space and it allows particle centers to align on the membrane length axis (x). In C4Pe10 membranes, the "pore protection phenomenon" is no longer detected, as due to membrane configuration there is no particle shift in the (y) direction. The distance between slots d_p allows particles to align in the x direction, however it is not enough for particle to reach the walls of the membrane surface. The resulting packing for C4Pe10 membrane appears higher than for the case of C4Pe7 units. The membrane surface is blocking is accentuated, the structure of the first layer tends to be regularly organized in a pyramidal structure similar to the body-centered cubic packing (Fig. 5c and d). The filtration cake formed for C4Pe10 units results consistently in less voids and a less porous cake first layers.

For the C4Pe20 units, particle distribution over the slots is similar to that observed for C4Pe10 units with no "pore protection phenomenon". The slot distance $d_p = 16$ µm is large enough and particles are optimally organized on the slots with their centers aligned in the membrane length axe. In addition, particles can deposit on the walls due to the larger distance between pores that allows the particles to arrange in random structures. This leads to more disorganized layers as shown in Fig. 5e and f. Since the structure is less conditioned by the membrane configuration, the hydrodynamics play a more important role in the arrangement of particles. The first arriving particles mainly block the slots and the following are driven by the fluid to the zones of the slots that are still open to the flow. This leads to a more complex and disorganized structure that could result in more compact cake layers.

The pore protection phenomenon and the existence of preferential arrangements depending on slots (or pore) distance were previously described. In the work by Ben Hassan et al. [17] using CLSM for direct observation of a thin cake (~35µm), it was possible to obtain evidence of particle organization patterns related to the ratio of particle size to distance between pores. Even if the membrane geometry is different in the current work, particles are initially and preferentially driven by the flow to the slots. The slot distribution affects how the membrane is blocked since particles with a size large compared to the distance between slots, protect neighboring slots from being blocked. It is thus evident that different membrane geometries affect pore blocking and particle arrangement. These effects persist to a certain degree into the later cake formation but they are attenuated as the system dynamics are later dominated by the cake growth rather than the membrane and the membrane geometry and the membrane-cake interaction (blocking) which explains the decreasing behavior of the porosity shown in Fig. 6.

3.2 Quantitative analysis

The filtration phenomenon is studied from the slot when particle blocking takes place, to the transition state where the dynamics are controlled by the membrane and the first layers of the deposit-. The pressure difference across the cake alone and the porosity evolution as a function of the deposited mass per unit of membrane surface throughout the filtration are represented in Fig. 6. The particle deposit formed on the C4Pe7 membrane exhibits a lower pressure difference than the cakes formed with the other filtration units. The C4Pe7 cake also undergoes a change of the pressure slope around $m = 55$ g/m². This change corresponds to the moment at which C4Pe7 and C4Pe10 porosity curves almost overlap and could suggest a rearrangement of the C4Pe7 cake structure into a more stable and compact organization. This possible particle rearrangement is consistent with the higher void fraction in the first layers previously discussed (Fig. 5 a and b). These voids could suffer a partial collapse, which may lead to the rise observed in the pressure drop. This could explain why the pressure values obtained for C4Pe7 membrane approach the values observed for the cake formed using C4Pe10 units. The pressure evolution corresponds is consistent with the qualitative description of the induced cake structure regarding the membrane geometry. As both cakes obtained with C4Pe7 and C4Pe10 membranes exhibit a similar pyramidal structure in the first layers, it is not surprising the agreement of the two curves with the collapse of the initial voids. The cake formed on the C4Pe10 membrane shows an intermediate behavior between the C4Pe7 and the C4Pe20. The pressure rise slope could suggest that the particle organization in the deposit is more stable than that obtained for C4Pe7 membrane and there is not a significant rearrangement of the particles as the pressure increases. A consistently higher pressure drop is observed for the C4Pe20 membrane cake. In this case, a more random particle arrangement within the first layers of the deposit could result in a more compact structure. The fluid drives particles to the remaining open filtering zones in the slots instead of spreading over the walls; therefore, for a deposited mass, the amount of particles blocking the flow through the slots can be higher for C4P20 membranes resulting in lower porosities and the elevated pressure drop.

It is also interesting to consider the later behavior when the cake layer growth is larger for the different slot width. Pressure drop is consistently lower for the cake formed on C4Pe7 membrane and higher for C4Pe20. This

difference suggests that the organized arrangement of particles in the first layers combined with the pore blocking have an effect on later cake structure and the mean porosity values. Membrane influence remains throughout the filtration experiments up to 70 g/m^2; nevertheless, further cake formation out of the studied range should drive the system dynamics to be determined by the cake.

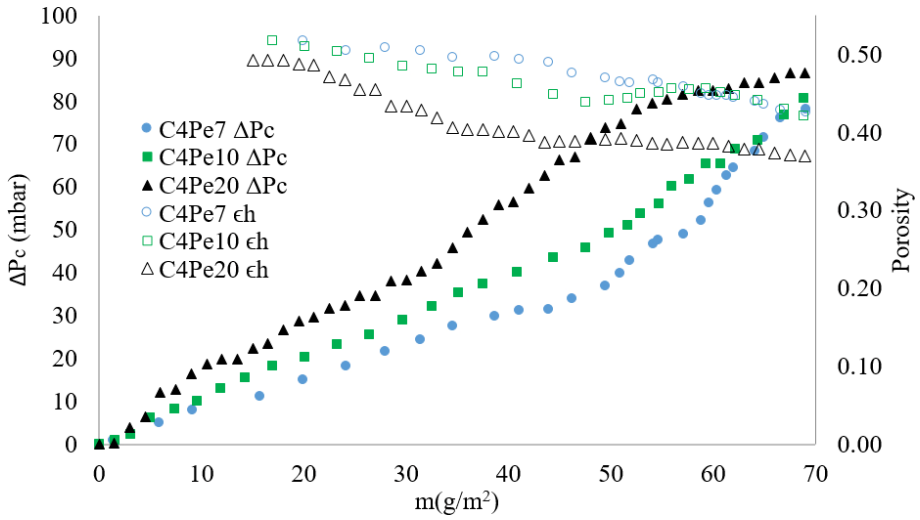

Fig. 6 Pressure drop across the cake alone and cake porosity behavior as a function of the deposited mass per surface unit.

The porosity values obtained in these experiments are comparable to the values usually reported for spherical particles. The work of Ouchiyama and Tanaka [26] used a simplified model to estimate the porosity of randomly packed spheres and found typical values of 0.43. In the work by Ben Hassan et al. [17] using different types of membranes, the effect of pore size and spacing on the cake porosity for a ~4 – 5 layers (~25 µm) was demonstrated. Porosity values of 0.41 and 0.49 were found for cakes of monodispersed particles (4.8 µm diameter) and for two different membranes. It was concluded that for smaller pore distance the pore protection phenomenon is enhanced and thus porosity is higher. Comparing with theoretical packing models, the porosity evolution for C4Pe7 and C4Pe10 membranes varies from loosest regular packing (cubic lattice: 6 points of contact per sphere) to loose random packing with theoretical porosities varying from 0.48 – 0.40, respectively. On the other hand, in the case of C4Pe20 membrane the porosity varies from loose random packing to close random packing (vibrated beds), corresponding to theoretical porosities of 0.40 – 0.36, respectively [27]. This confirms the previous qualitative analysis of the cake structure and particle organization obtained for the different membrane geometries. It can be noticed that in these experiments the theoretical densest regular packing (porosity ~0.26) is never reached.

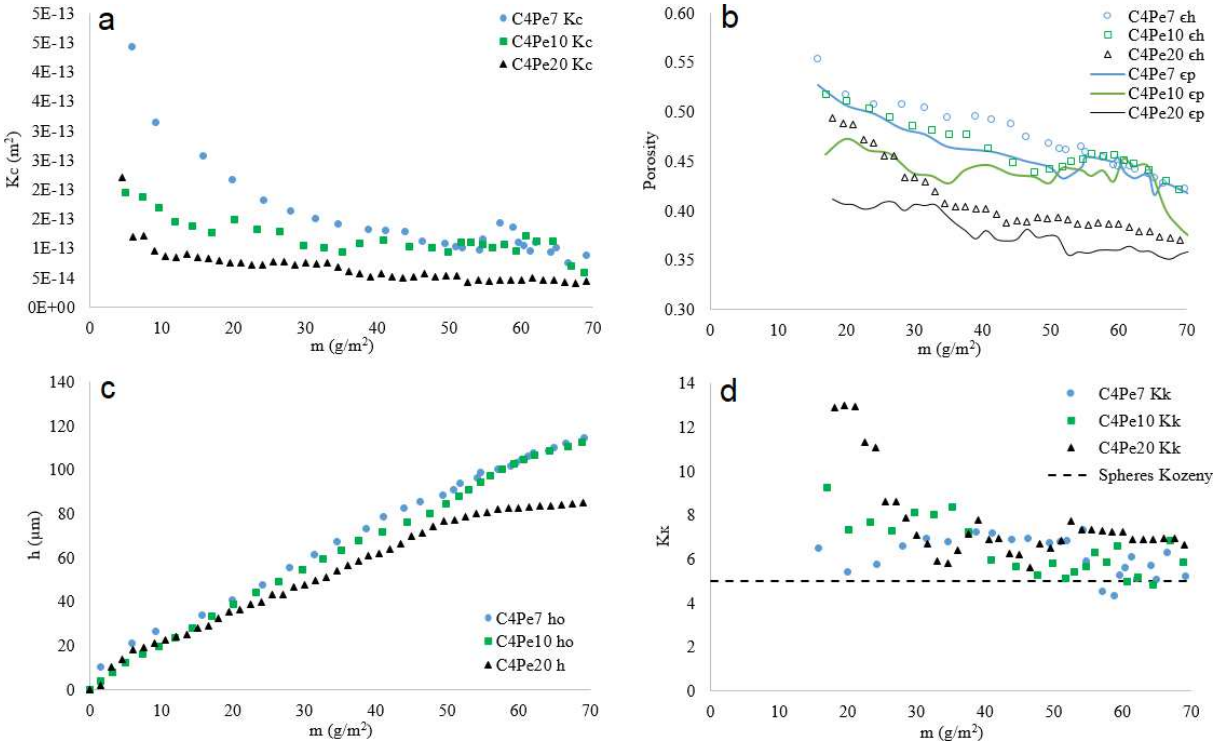

Fig. 7 a) Permeability of the cake. b) Porosity ϵ_h estimated using Eq. 2 (○ C4Pe7, □ C4Pe10, Δ C4Pe20) and Darcy's equation ϵ_p (Color solid lines) for the different membranes. c) Mean cake height. d) Estimated Kozeny coefficient. All the graphics are plotted as function of the deposited mass per membrane surface unit.

Fig. 7a shows the variations of the cake permeability as a function of the deposited mass per membrane surface unit. The cake permeability ($K_c = \bar{h}/R_c$) is calculated from the cake resistance. The cake hydraulic resistance is obtained from the difference of the total and the membrane resistance ($R_c = R_t - R_m$). The cake resistance allows definition of the permeability resulting from the cake and the membrane blocking. These two resistance components can be observed in the permeability evolution which exhibits an important decrease as the first layers are formed. The initial sharp decrease can be related to the slot blockage phenomenon. This can be confirmed from the variation of cake height as a function of the deposited mass (Fig. 7c) for which 10 g/m^2 corresponds to 15 µm of cake height. With regards to particle size this corresponds to the second layer formation. The later permeability becomes gradually more influenced by the further cake growth and decreases toward a stable value. This corresponds to the previous qualitative explanation, which suggests a possible particle rearrangement in the deposits as the pressure rises. The differences in the initial permeability values are explained by two main features: the partial blocking phenomenon and the induced cake structure. For C4Pe7 membranes the initial permeability is higher and this is related to the geometry and the accentuated slot blockage by the particles for C4Pe10 and C4Pe20 units. The later cake build-up controls the permeability behavior as it approaches a stable value. In the case of C4Pe10 and C4Pe20 units the absence of the "pore protection" phenomenon (Fig. 5c and d) results in a lower permeability than C4Pe7. As the cake formation continues in C4Pe10 units the permeability becomes stable around the same values as found for C4Pe7. This is consistent with the porosity evolution that overlaps for C4Pe7 and C4Pe10 around 55 g/m² and it is also confirmed by a lower permeability corresponding to a lower porosity for C4Pe20 membrane.

To provide a more complete characterization of the fouling mechanisms, the porosity ϵ_h estimated using Eq. 2 is compared with the porosity ϵ_p calculated using Eq. 3 with $K_K = 5$. Fig. 7b shows both ϵ_h and ϵ_p represented by symbols and solid lines respectively. These two estimates of the porosity exhibit a similar behavior for the cakes formed under the different membrane configurations; however the values differ slightly, with ϵ_p consistently lower than ϵ_h. This difference could be explained by the assumption of a constant value for K_K when calculating ϵ_p. Previous work has reported the dependence of the K_K on the porosity [28]. Although the Kozeny-Carman formula provides a semiempirical relation for the permeability, analytical development of the equations of continuity and momentum for creeping flow has been made. Snyder and Stewart [29] solved creeping flow through a loose cubic packing ($\epsilon = 0.476$) and dense cubic packing ($\epsilon = 0.26$) media of uniform

spheres. Their solutions show a fair agreement with the Kozeny-Carman equation, finding K_K values of 4.16 and 4.86, for the high and low porosity media respectively. Vidal et al. [30] performed massive parallel Lattice-Boltzmann simulations of flow through monodispersed and highly polydispersed spherical particle packing using Monte-Carlo methods. Their results show a reasonable good agreement with Carman-Kozeny formula. For monodispersed particles, they obtained K_K values ranging from 5.5 to 6.0 for high (ϵ = 0.46) and low (ϵ = 0.38) cake porosities respectively. The experimental results for ϵ_h and the previous literature results show good agreement and validate the current estimation regardless of the slight differences with ϵ_p.

Considering K_K variable as a function of the porosity, Eq. 3 is used to calculate the values for each estimated porosity ϵ_h. In Fig. 7d, K_K varies within a consistent range: for the three geometries they are close to but generally above the typical value of K_K = 5 for monodispersed spheres. For C4Pe7 and C4Pe10 filtration cakes, K_K exhibits barely an evolution with mean values of 6.0 and 6.6 respectively; for C4Pe20, K_K starts at a high value and decreases towards a stabilization around ~7. In the noted prior studies [29], [30], lower porosities lead to higher K_K, which is also the case for the current experiments.

3.3 Numerical simulation

As described in Section 2.5, three geometries were studied in order to analyze membrane blocking when the first cake layers are forming and confirm the experimental results. Following findings previously described in the literature, a uniform cake surface is expected when the filtration has already taken place and the filtration dynamics are controlled predominantly by the cake rather than the membrane; however in the first stages of the filtration, membrane permeability gradients could influence the first layers formation[31]. In the case of these simulations as shown in Section 2.5, an optimal coverage of the membrane is studied, corresponding to the sketches of Fig. 4d, e and f. The results of the qualitative analysis helped to define the simplified model geometries for the simulations (Fig. 5). The pressure drop across the system for the three simulated geometries is calculated, and from this value the contributions to the total resistance are determined(R_m and R_c).

The simulation results allow calculation of the hydraulic resistance of the first layer of particles (blocking layer), which are responsible for the partial blocking of the membrane. In order to compare the hydraulic resistance caused by the first layer with the experimental results obtained for ~3 layers, the mean height of the blocking layer is calculated taking into account the geometry of the membrane (specifically *Pe*), indeed the number of particle blocking the slots depends on the numbers of slots per unit of area. For this reason, the blocking layer height for the three geometries is not the same and the lowest value of *Pe* (C4Pe7) yields a larger mean height of the blocking layer; for higher slot distance (C4Pe20) there are fewer pores and hence less particles deposited, and this contributes to make the blocking layer height smaller. It must be pointed out that the mean height of the blocking layer for all the membrane configurations is lower than the particle diameter (8.4 µm). The particle penetration inside the slot also contributes to this feature. As these simulations were run only for the blocking layer, only one pair of data was obtained for each membrane configuration.

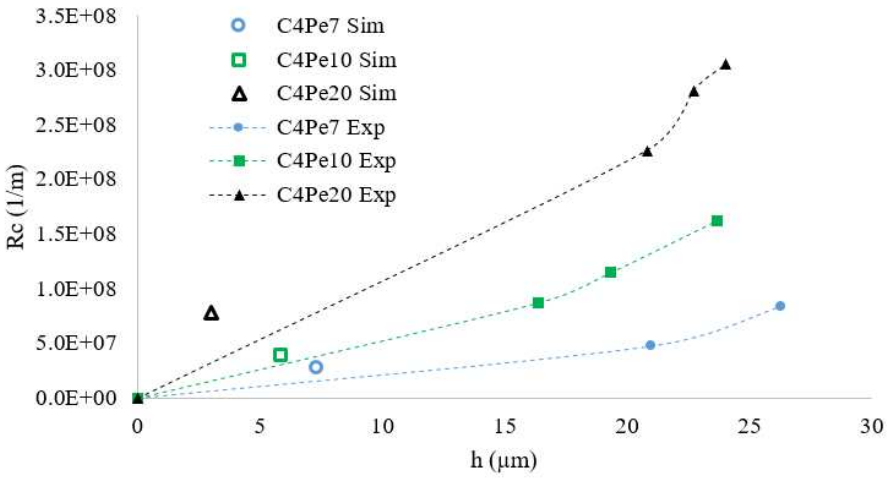

Fig. 8 Experimental values of the cake-blocking hydraulic resistance for the different membrane geometries when the initial layers are forming (dashed lines with filled symbols). Hollow symbols represent the simulated resistance due to particles blocking the slots.

Fig. 8 shows the comparison of the simulated (1 layer) and the experimental (~ 3 layer) hydraulic resistance caused by the cake and the membrane blocking as a function of the deposit height at the beginning of the filtration. Hollow symbols represent the simulation results for the cake hydraulic resistance when the slots are optimally blocked for each membrane geometry. The values are plotted as a function of the mean height for the corresponding geometry. Note the proximity of the simulation results with the respective experimental curve at the early membrane blocking (1 layer ~3-7 µm height depending on the membrane geometry). This indicates that the experimental data is in a consistent range. There is a difference in the resistance obtained from the simulations for the different geometries. This could be explained by the assumption of an optimal blocking of the slots by the particles; this is not always the case in the real experiments as some flow streamlines are closer to the membrane walls than a particle radius. This promotes particles to deposit on the wall before reaching a pore and is likely a reason why the simulations are displaced from the experimental curves.

Nevertheless, these simulations provide a means of rationally evaluating the qualitative description of the membrane blocking in order to compare with the quantitate analysis of the experiments. Indeed, the qualitative analysis remains subject to the interpretation of 2D images, which leads to an uncertainty in the depth direction. However, as the simulated 3D geometry is based on the qualitative description, the calculations obtained from the simulations confirms the consistency of the approach as there is a fair agreement with the experimental results.

4 Conclusion

The proposed *in-situ* and real-time experiment based on the design and construction of a new micro-system combine with the analysis methodology are found to be of significant utility for characterizing the first stage of the filtration process of micrometric particles. The cake growth and its organization are analyzed though the CGM, which tracks the cake surface during filtration. The cake mean height is analyzed with the concentration and velocity calculations to check the mass balance. An additional qualitative analysis is performed to characterize the structure of the first particle layers. The observations are used to describe the cake structure and define the geometry for the simulations.

The filtration performance for the different membrane geometries appear to be quite similar, but the pressure drop can be affected by the distance between slots. The initial particle arrangement is notably conditioned by the membrane geometry that has also an influence on pore blocking and further cake growth, which influences the pressure drop differences. The numerical simulations provide a means of rationally evaluating the role of the membrane geometry and the first blocking particles on the deposit formed at the membrane. The simulation results for the blocking layer hydraulic resistance are in agreement with the experimental data for the current suspension. The qualitative and quantitative analysis conclude on the effect of membrane geometry on “pore blocking” and permeability reduction. The size and the distance between slots as well as the particle diameter play a role on the “pore protection phenomenon”. These conclusions can be applied to real industrial applications by characterizing industrial membrane filtration units (cylindrical pores instead of slots) using the crucial parameters pointed out in this study, the size of the slot/pore and the distance between two neighbor slots/pores. This could lead to a better choice of membrane units depending on the material to be retained. The optical set-up designed for this study and analysis techniques developed are interesting tools that could be adapted to provide *in-situ* and real time information to perform deeper analysis for different filtration conditions, like for example crossflow filtration.

Acknowledgments

This work was done in the frame of the research grant program AAP 2015 from Idex UNITI “NEMESIS” conv-ANR-11Idex-0002-02.

The authors thank Pierre Joseph from the « Laboratoire d'analyse et d'architecture des systèmes » (LAAS).

References

[1] C. Charcosset, “Procédés membranaires à application pharmaceutique et biotechnologique,” *ITBM-RBM*, vol. 27, no. 1, pp. 1–7, Feb. 2006.

[2] A. Grelot, R. K. Dereli, F. P. van der Zee, J. G. M. van der Lubbe, and B. Heffernan, “Performances of Anaerobic Membrane Bioreactors Treating Thin Stillage from Bioethanol Plants at Different Sludge Retention Times,” *Procedia Eng.*, vol. 44, pp. 776–779, 2012.

[3] L. Qin *et al.*, “Anoxic oscillating MBR for photosynthetic bacteria harvesting and high salinity wastewater treatment,” *Bioresour. Technol.*, vol. 224, pp. 69–77, Jan. 2017.
[4] N. Vasileva, Y. Ivanov, S. Damyanova, I. Kostova, and T. Godjevargova, “Hydrolysis of whey lactose by immobilized β-galactosidase in a bioreactor with a spirally wound membrane,” *Int. J. Biol. Macromol.*, vol. 82, pp. 339–346, Jan. 2016.
[5] T. Kudra, “FILTERS AND FILTRATION HANDBOOK 4th Edition (1997) By T. Christopher Dickenson Publisher: Elsevier Advanced Technology The Boulevard, Langford Lane, Kidlington, Oxford OX5 1GB, U.K.,” *Dry. Technol.*, vol. 17, no. 1–2, pp. 363–364, Jan. 1999.
[6] P. Schmitz, B. Wandelt, D. Houi, and M. Hildenbrand, “Particle aggregation at the membrane surface in crossflow microfiltration,” *J. Membr. Sci.*, vol. 84, no. 1, pp. 171–183, Sep. 1993.
[7] S. Xue, C. Li, J. Li, H. Zhu, and Y. Guo, “A catechol-based biomimetic strategy combined with surface mineralization to enhance hydrophilicity and anti-fouling property of PTFE flat membrane,” *J. Membr. Sci.*, vol. 524, pp. 409–418, Feb. 2017.
[8] J. Liu, Z. Liu, X. Xu, and F. Liu, “Saw-tooth spacer for membrane filtration: Hydrodynamic investigation by PIV and filtration experiment validation,” *Chem. Eng. Process. Process Intensif.*, vol. 91, pp. 23–34, May 2015.
[9] E. Iritani, N. Katagiri, and G. Inagaki, “Compression and expansion properties of filter cake accompanied with step change in applied pressure in membrane filtration,” *Sep. Purif. Technol.*
[10] J. Mendret, C. Guiguir, C. Cabassud, and P. Schmitz, “Dead-end ultrafiltration and backwash: dynamic characterisation of cake properties at local scale,” *Desalination*, vol. 199, no. 1, pp. 216–218, Nov. 2006.
[11] W. D. Mores and R. H. Davis, “Direct visual observation of yeast deposition and removal during microfiltration,” *J. Membr. Sci.*, vol. 189, no. 2, pp. 217–230, Aug. 2001.
[12] J. Altmann and S. Ripperger, “Particle deposition and layer formation at the crossflow microfiltration,” *J. Membr. Sci.*, vol. 124, no. 1, pp. 119–128, Feb. 1997.
[13] T. Schluep and F. Widmer, “Initial transient effects during cross flow microfiltration of yeast suspensions,” *J. Membr. Sci.*, vol. 115, no. 2, pp. 133–145, Jul. 1996.
[14] P. H. Hodgson, V. I. Pillay, and A. G. Fane, “Visual study of crossflow microfiltration with inorganic membranes: resistance of biomass and particulate cake.” 1993.
[15] H. Li, A. G. Fane, H. G. L. Coster, and S. Vigneswaran, “Direct observation of particle deposition on the membrane surface during crossflow microfiltration,” *J. Membr. Sci.*, vol. 149, no. 1, pp. 83–97, Oct. 1998.
[16] Y. P. Zhang, A. W. K. Law, and A. G. Fane, “Determination of critical flux by mass balance technique combined with direct observation image analysis,” *J. Membr. Sci.*, vol. 365, no. 1, pp. 106–113, Dec. 2010.
[17] I. Ben Hassan, C. Lafforgue, A. Ayadi, and P. Schmitz, “In situ 3D characterization of monodispersed spherical particle deposition on microsieve using confocal laser scanning microscopy,” *J. Membr. Sci.*, vol. 454, pp. 283–297, Mar. 2014.
[18] P. Le-Clech, Y. Marselina, Y. Ye, R. M. Stuetz, and V. Chen, “Visualisation of polysaccharide fouling on microporous membrane using different characterisation techniques,” *J. Membr. Sci.*, vol. 290, no. 1–2, pp. 36–45, Mar. 2007.
[19] T. van de Laar, S. ten Klooster, K. Schroën, and J. Sprakel, “Transition-state theory predicts clogging at the microscale,” *Sci. Rep.*, vol. 6, p. 28450, Jun. 2016.
[20] I. Ben Hassan, C. Lafforgue, C. Ellero, A. Ayadi, and P. Schmitz, “Coupling of local visualization and numerical approach for particle microfiltration optimization,” *Microsyst. Technol.*, vol. 21, no. 3, pp. 509–517, Mar. 2015.
[21] J. Mendret, “Mise au point de méthodes de caractérisation non destructives du colmatage de membranes : application à la caractérisation in situ d’un dépôt particulaire en ultrafiltration frontale en lien avec les performances du procédé,” thesis, Toulouse, INSA, 2007.
[22] M. Honkanen, P. Saarenrinne, T. Stoor, and J. Niinimäki, “Recognition of highly overlapping ellipse-like bubble images,” *Meas. Sci. Technol.*, vol. 16, no. 9, p. 1760, 2005.
[23] C. A. Acuña and J. A. Finch, “Tracking velocity of multiple bubbles in a swarm,” *Int. J. Miner. Process.*, vol. 94, no. 3, pp. 147–158, Apr. 2010.
[24] Carman, “Fluid flow though granular beds,” *Chemical Engineering Research and Design*, pp. 415–421, 1937.
[25] P. K. Kundu, I. M. Cohen, and D. R. Dowling, Eds., “Chapter 9 - Boundary Layers and Related Topics,” in *Fluid Mechanics (Fifth Edition)*, Boston: Academic Press, 2012, pp. 361–419.
[26] N. Ouchiyama and T. Tanaka, “Porosity estimation for random packings of spherical particles,” *Ind. Eng. Chem. Fundam.*, vol. 23, no. 4, pp. 490–493, Nov. 1984.
[27] F. A. L. Dullien, *Porous Media: Fluid Transport and Pore Structure*. Academic Press, 2012.
[28] M. A. Knackstedt and X. Zhang, “Direct evaluation of length scales and structural parameters associated with flow in porous media,” *Phys. Rev. E*, vol. 50, no. 3, pp. 2134–2138, Sep. 1994.

[29] L. J. Snyder and W. E. Stewart, “Velocity and pressure profiles for Newtonian creeping flow in regular packed beds of spheres,” *AIChE J.*, vol. 12, no. 1, pp. 167–173, Jan. 1966.
[30] D. Vidal, C. Ridgway, G. Pianet, J. Schoelkopf, R. Roy, and F. Bertrand, “Effect of particle size distribution and packing compression on fluid permeability as predicted by lattice-Boltzmann simulations,” *Comput. Chem. Eng.*, vol. 33, no. 1, pp. 256–266, Jan. 2009.
[31] J. Mendret, C. Guigui, C. Cabassud, and P. Schmitz, “Numerical investigations of the effect of non-uniform membrane permeability on deposit formation and filtration process,” *Desalination*, vol. 263, no. 1, pp. 122–132, Nov. 2010.

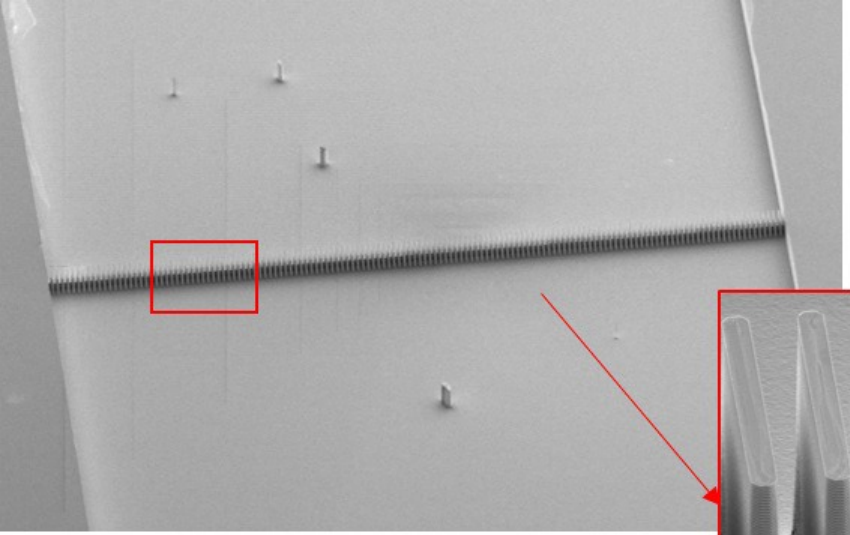

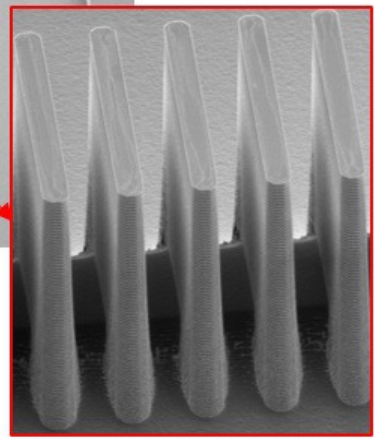

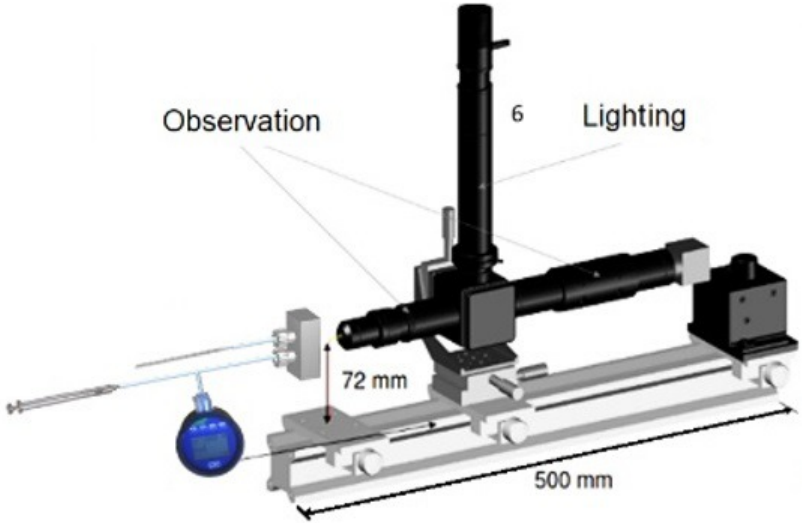
Observation
6
Lighting
72 mm
500 mm

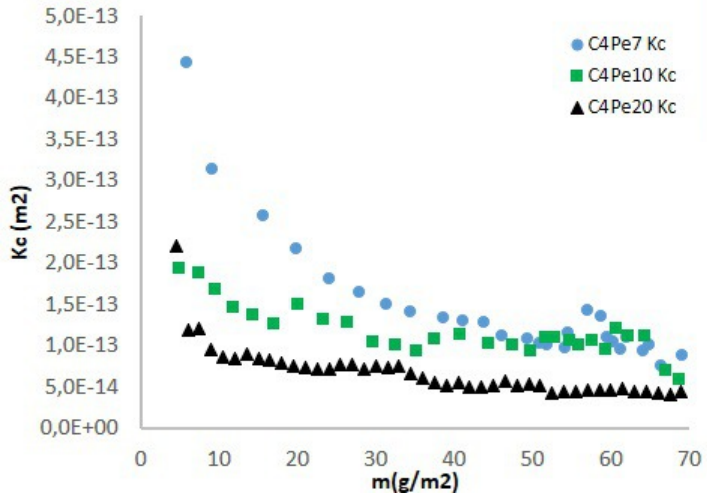
5,0E-13
4,5E-13
4,0E-13
3,5E-13
3,0E-13
2,5E-13
2,0E-13
1,5E-13
1,0E-13
5,0E-14
0,0E+00
Kc (m2)
0
10
20
30
40
50
60
70
m(g/m2)
C4Pe7 Kc
C4Pe10 Kc
C4Pe20 Kc